Journal of Japan Association for Earthquake Engineering, Vol. 22, No. 3, 2022

CONTROL PERFORMANCE DIAGRAMS FOR TUNED MASS DAMPERS MOUNTED ON INELASTIC REINFORCED CONCRETE BUILDINGS

Kensaku KANEKO[1], Kazuhisa TAKAHASHI[2], Kaiwei ZHANG[3], Tsung-Wu CHEN[4], Bo-Han LEE[5] and Chun-Chung CHEN[6]

[1] Member, Dr. Eng., Lecturer, Osaka Metropolitan University, kanekok@omu.ac.jp
[2] Member, M. Eng., Former graduate student, Tokyo Institute of Technology, takahashi.k@shimz.co.jp
[3] M. Eng., Kozo Keikaku Engineering Inc., kaiwei-zhang@kke.co.jp
[4] Ph.D., Kuochen and Associates Ltd., alex@kc.ctntu.com
[5] Ph.D., Assistant Research Fellow, National Center for Research on Earthquake Engineering, bhlee@narlabs.org.tw
[6] Ph.D., Associate Researcher, National Center for Research on Earthquake Engineering, jingochen@narlabs.org.tw

ABSTRACT: This paper describes a design method for tuned mass dampers (TMDs) that reduce seismic responses in reinforced concrete buildings. To reduce the seismic responses to a wide range of strong ground motions, displacement-dependent optimal tuning ratios of linear TMDs are formulated for nonlinear responses. Performance curve diagrams are proposed using the optimal tuning ratios determined by nonlinear time history analyses with various mass ratios and damping ratios. These diagrams allow us to visually determine the appropriate TMD under the constraints of its mass, damping coefficient, and peak deformation.

Keywords: *Mass damper, Tuning ratio, Nonlinear response, Control performance, Time-history analysis*

1. INTRODUCTION

Since the early 2010s, heavy tuned mass dampers (TMDs) have been actively developed to reduce the seismic responses of existing tall buildings in Japan[1)–3)]. These seismic rehabilitation measures are intended to protect against long-period ground motions. Many researchers have noted that the possible future Great Nankai Trough Earthquake would have long-period ground motions that could cause severe damage to tall buildings in Japan. Installing TMDs on rooftops is advantageous for buildings with limited installation space and has attracted attention from many structural engineers and researchers. A heavy TMD can reduce seismic responses to strong ground motions even with far shorter duration than

wind disturbance. Advanced TMDs have been studied for additional earthquake protection, including multiple TMDs[4], building mass dampers[5], and displacement dependent TMDs[6]. Semi-active control methods with friction based TMDs[7, 8] also fall into this category. Although these advanced technologies may permit higher control effects, a conventional passive TMD with linear viscous elements can still achieve low-cost seismic rehabilitation without these technologies[9]. Furthermore, the connections between rooftop TMDs and buildings are simpler than those of other dampers installed on several floors. In this respect, TMDs are suitable for seismic rehabilitation in countries with insufficient damping technology.

Despite these potential technologies, few studies have addressed the effects of using a TMD with a linear viscous damper on reinforced concrete buildings during strong ground motions. A TMD tuned to the initial stiffness of the building may have reduced control performance due to the strong nonlinearity of processes such as crack formation in the concrete or the yielding of reinforcing bars. This issue has motivated the development of advanced TMDs that enhance their robustness to changes in natural frequency. In terms of passive control methods, a typical approach involves using multiple TMDs with different natural frequencies, which were originally studied to account for stiffness uncertainties. Semi-active control methods with variable damping coefficients have also been studied to address time-dependent nonlinearity[10]. However, it is uncertain how the structural properties of a linear TMD should be selected to maximize control performance for moderate-to-strong ground motions. Clarifying this fundamental problem can advance TMD technologies.

This paper investigates the control performance of conventional TMDs with linear viscous elements for reinforced concrete buildings. The objectives include finding a reasonable TMD stiffness for reducing seismic responses to moderate-to-strong ground motions and presenting graphical solutions with multiple constraints, including the allowable TMD deformation. In addition, nonlinear time-history analyses using a spatial frame model demonstrate the usefulness of the proposed design method.

2. ANALYSIS METHODS FOR GENERATING CONTROL PERFORMANCE DIAGRAMS

2.1 Controlled buildings and input ground motions

Consider TMDs installed into reinforced concrete buildings with five, ten, and 14 stories. The TMDs mounted on the rooftops have physical properties including mass m_a, stiffness k_a, and damping coefficient c_a (Fig. 1). The mass m_a is normalized by the first effective mass of the building M_b^{eff} as

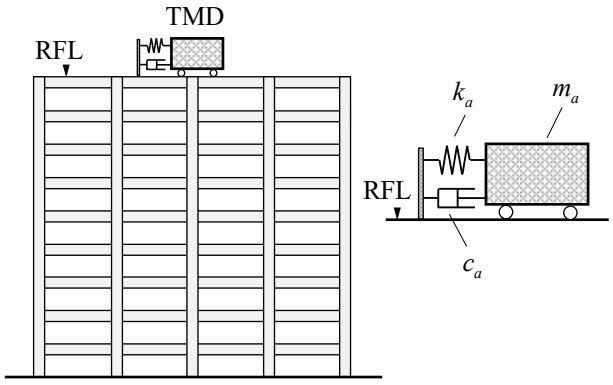

Fig. 1 Controlled building

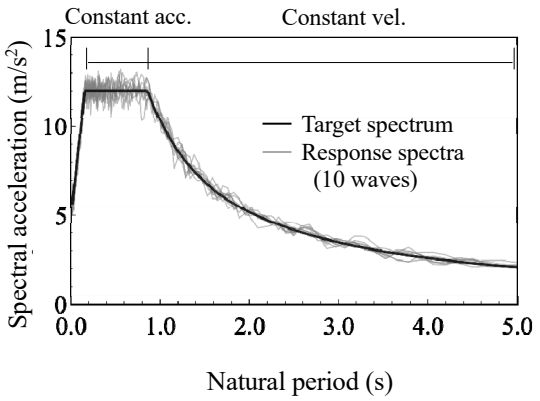

Fig. 2 Response spectra for a 5% damping ratio

follows:

$$\mu = m_a / M_b^{eff} \tag{1}$$

The mass ratio μ is assumed to be $0.02 \le \mu \le 0.1$ to ensure appropriate seismic effectiveness.

Simulated and recorded ground motions were employed to investigate several of the objectives. The simulated motions were generated so that their response spectra matched the specified target spectrum (Fig. 2). The target spectrum is referred to the class II soils specified in the Japanese Ministry of Construction Notification. An amplitude envelope with a duration of 120 s and a random phase angle accompanied by Fourier amplitudes generated ten time-history acceleration samples, which gives the response spectra shown in Fig. 2. The simulated ground motions were used to generate the control performance diagrams shown in Section 4. Subsequently, recorded ground motions were selected to demonstrate the TMD control performance for three typical buildings.

2.2 Analysis models

This study employs a two-degree-of-freedom (2-DOF) lumped mass model (Fig. 3). Evaluating the control performance requires many time-history analyses, and the 2-DOF model is appropriate because of its low numerical cost. By combining a well-known equivalent single-degree-of-freedom (SDOF) building and the TMD, 2-DOF systems are presented in a mathematical form involving the displacement compatibility. Letting ψ be the nondimensional value that is computed by a participation factor multiplied by the first modal vector element corresponding to the TMD position, an exact equation of motion is derived in the following form:

$$\mathbf{M}\ddot{\mathbf{U}} + \left(\mathbf{C}_b + \mathbf{C}_a\right)\dot{\mathbf{U}} + \mathbf{K}_a\mathbf{U} + \mathbf{Q}(\mathbf{U}) = -\mathbf{M}\mathbf{r}\ddot{u}_g \tag{2}$$

where the vectors and matrices are defined by

$$\mathbf{M} = \begin{bmatrix} \psi^2 m_a & 0 \\ 0 & M_b^{eff} \end{bmatrix}, \quad \mathbf{C}_b = \begin{bmatrix} 0 & 0 \\ 0 & C_b \end{bmatrix}, \quad \mathbf{C}_a = \psi^2 c_a \begin{bmatrix} 1 & -1 \\ -1 & 1 \end{bmatrix}, \quad \mathbf{K}_a = \psi^2 k_a \begin{bmatrix} 1 & -1 \\ -1 & 1 \end{bmatrix} \tag{3a–d}$$

$$\mathbf{U} = \begin{Bmatrix} u_a \\ U \end{Bmatrix}, \quad \mathbf{r} = \begin{Bmatrix} 1 \\ \psi \end{Bmatrix}, \quad \mathbf{Q} = \begin{Bmatrix} 0 \\ \psi Q(q) \end{Bmatrix}, \quad U = \psi q \tag{3e–h}$$

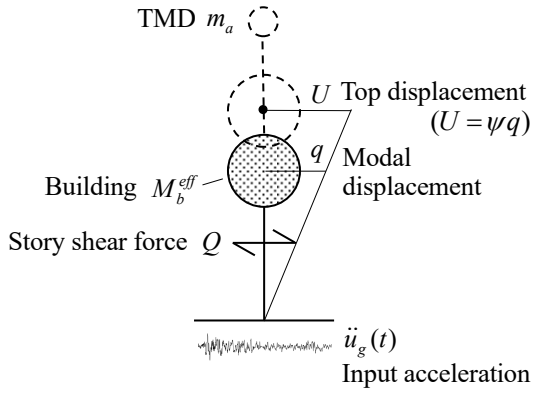

Fig. 3 Equivalent 2-DOF system for a building and TMD

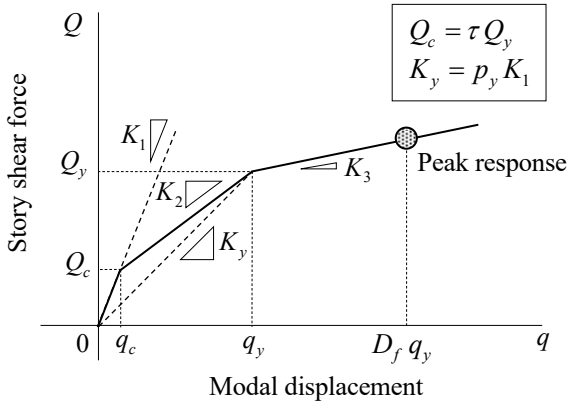

Fig. 4 Envelope curve of an equivalent SDOF system for a building and TMD

using the displacements U, q, and u_a as shown in Fig. 3. The symbols Q and C_b are the restoring shear force and damping coefficient of a SDOF building, respectively (Fig. 4). By scaling the stiffness and strength shown in Eq. (3), the response error arising from the dimensionality reduction can be negligibly small. The errors were confirmed to be within 5% of the original multi-degree-of-freedom system if the first mode shape held during an elastic-plastic response[9].

To apply structural properties to Eq. (3), the concrete building was assumed to have ten stories, a floor height of 3.0 m, and an inverted triangle mode shape ($\psi = 1.5$). By using the building height H (m), the initial natural period T_1 (s) was calculated from an empirical formula ($T_1 = 0.02H$). The ratio of the base shear strength Q_y to the building total mass was 0.35. These specific values do not lose generality because all the values, including tuning parameters and peak responses, have dimensionless forms in the later discussion. In other words, any structural properties are applicable to the results obtained from this study. The restoring force Q follows the Sozen-Takeda degrading rule with a trilinear envelope[11] where the post-yield stiffness K_3 is 1/100 times the initial stiffness K_1. The inner loop unloading stiffness reduction factor is considered 0.4. Non-dimensional parameters p_y and τ are the normalized stiffness and strength, defined as follows:

$$p_y = \frac{K_y}{K_1}, \qquad \tau = \frac{Q_c}{Q_y} \tag{4a, b}$$

where K_y is the secant stiffness at a yield point. The symbols Q_c and Q_y are the first and second strength points on the envelope, as shown in Fig. 4. Once the initial natural period T_1 was determined, the two parameters p_y and τ give a unique envelope curve in non-dimensional axes (ductility factor versus story shear coefficient).

Equation (2) is solved by direct time-history analysis with the Newmark β scheme, with an incremental time step of 1/1000 s. The overall damping ratio of 0.03 is incorporated into the building as proportional type tangent stiffness. The reference frequency was based on the first vibration mode without the TMD.

3. TUNING METHOD FOR MODERATE-TO-STRONG GROUND MOTIONS

3.1 Optimal tuning ratio for specific seismic intensity

The tuning parameters contain the mass, stiffness, and damping ratio of the TMD. The optimal stiffness and damping ratio are discussed here, and the mass is addressed in Section 4.

For determining the optimal stiffness k_a, the tuning ratio γ is determined as follows:

$$\gamma = \frac{\omega_a}{\omega_b}, \qquad \omega_a = \sqrt{\frac{k_a}{m_a}} \tag{5a, b}$$

where γ is defined as the ratio of the eigen circular frequencies for the building ω_b and for the TMD ω_a. If the building responds in its elastic range, the closed form of the optimal tuning ratio only depends on the mass ratio. Applying white-noise motion to the building base leads to the following well-known formula[12]:

$$\gamma_e^* = \frac{\sqrt{1 - \bar{\mu}/2}}{1 + \bar{\mu}}, \qquad \bar{\mu} = \psi^2 \mu \tag{6a, b}$$

Seismic responses over the elastic limit require a modification to Eq. (6) because the equivalent natural frequency significantly changes in the controlled building. Kaneko et al.[9] proposed the following

optimal tuning equation depending on the nonlinearity of the building:

$$\gamma_p^* = \frac{1}{\alpha(D_f^*)}\gamma_e^* \tag{7}$$

$$D_f^* = 0.5D_f\,, \qquad \frac{1}{\alpha(D_f^*)} = \begin{cases} 1 & \text{if } D_f^* < D_c \\ \sqrt{\dfrac{p_y}{D_f^*}}\sqrt{\tau + (D_f^* - D_c)\dfrac{1-\tau}{1-D_c}} & \text{if } D_c \le D_f^* < 1 \\ \sqrt{\dfrac{p_y}{D_f^*}} & \text{if } D_f^* \ge 1 \end{cases} \tag{8a, b}$$

where the ductility factor D_f should be evaluated for the building without the TMD. Although this equation is based on the secant stiffness at peak displacement, Eq. (8) involves a minor modification. The empirical coefficient of 0.5 was identified through numerical optimizations with many nonlinear time-history analyses. While the stiffness ratio p_y strongly affects the optimal tuning ratio γ_p^* (Fig. 5(b)), the difference of γ_p^* in terms of the strength ratio τ is negligible (Fig. 5(a)), especially for $D_f > 1$. Considering typical values used in Japan, only a τ of 0.3 was employed in the later results.

The optimal damping coefficient c_a can be evaluated from the optimal damping ratio h_a:

$$c_a = 2m_a h_a \omega_a \tag{9}$$

For elastic responses, the optimal damping ratio that corresponds to Eq. (6) is expressed as[12]:

$$h_{a,e}^* = \frac{1}{2}\sqrt{\frac{\bar{\mu}(1-\bar{\mu}/4)}{(1+\bar{\mu})(1-\bar{\mu}/2)}} \tag{10}$$

The optimal damping ratio has approximately the same form as Eq. (10):

$$h_a^* \approx h_{a,e}^* \tag{11}$$

3.2 Indices of optimal TMDs and some constraints

With these optimal tuning parameters, control performance was evaluated using the reduction ratio of peak displacement:

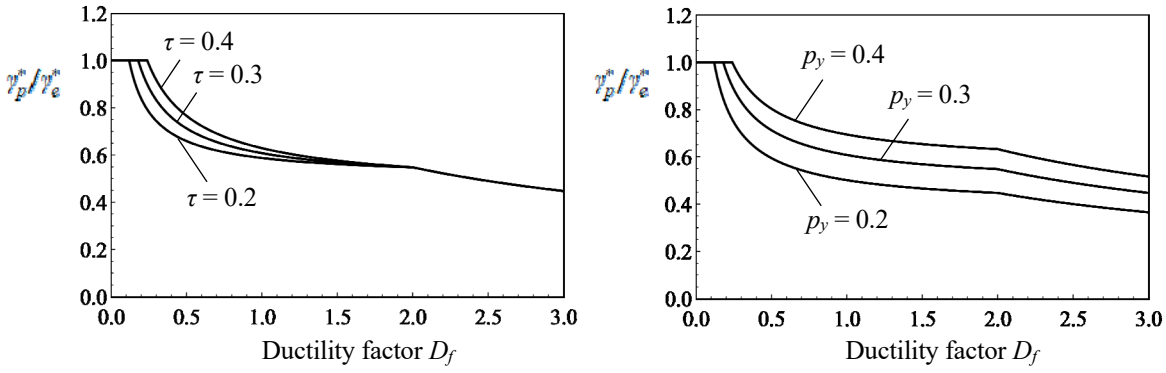

(a) Effect of strength ratio (b) Effect of stiffness ratio

Fig. 5 Normalized tuning ratios for nonlinear buildings

$$R_d = \frac{\max_t |U(t)|}{\max_t |U_0(t)|} \tag{12}$$

where U_0 and U are the peak displacement of the uncontrolled and controlled buildings, respectively. In Fig. 6, the lower limit of R_d is summarized using a variable TMD stiffness tuned to the evolved D_f. Nevertheless, the reduction ratio R_d becomes larger as D_f evolves because the uncontrolled buildings are gradually damped by hysteretic energy. Furthermore, the actual R_d becomes larger than the lower limit because the TMD stiffness cannot be changed.

Other constraints also reduce control performance. The TMD damping coefficient may require far larger values than the optimal value. Its damper stroke is still large compared to the other damped structures and may reach its tolerance during strong ground motions. To investigate the damper stroke, the normalized deformation of the TMD was defined as follows:

$$d(t) = u_a(t) - U(t), \quad \chi = \frac{\max_t |d(t)|}{\max_t |U(t)|} \tag{13a, b}$$

where χ is independent of the initial natural period or the building height. For elastic responses, the normalized deformation χ is accurately estimated by the following expression[5]:

$$\chi_e^* = \frac{1}{\sqrt{2\bar{\mu}}} + 0.83\sqrt{\bar{\mu}} \tag{14}$$

Figure 7 shows the normalized deformation χ during nonlinear responses, which can be approximately constant for $D_f \geq 1$. This assumption suggests selecting a specified χ for $D_f = 1$ to generate the control performance diagrams addressed in Section 4.

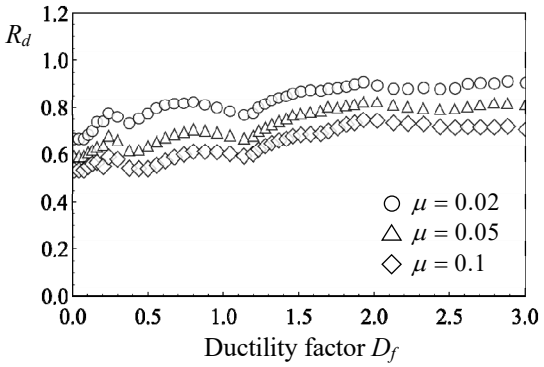

Fig. 6 Displacement reduction ratio depending on ductility factor

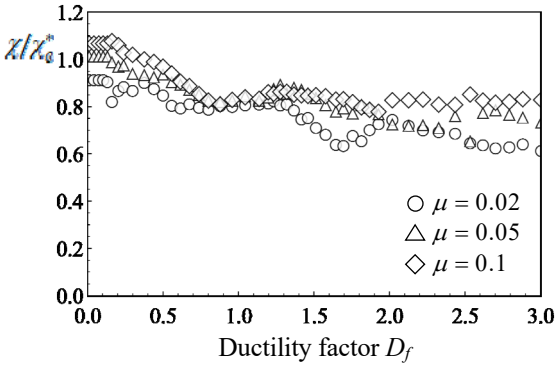

Fig. 7 TMD deformation depending on ductility factor

3.3 Practical tuning methods for several seismic intensities

As Eq. (7) implies, the linear TMD tuned to strong ground motions is not optimal for moderate ground motions. There exists an inevitable R_d trade-off among different seismic intensities. We thus need to select only one reference seismic intensity so that a desirable R_d is achieved over a wide range of D_f values. This complex tuning can be avoided by an alternative method based on a reasonable criterion discussed in the following paragraph.

Consider the three states of cracking, yielding, and the ultimate state; $R_{d,c}$, $R_{d,y}$, and $R_{d,u}$ denote

the minimized reduction ratio at each state, respectively:

$$R_{d,c}(\gamma) = R_d(\gamma; D_f = D_c) \qquad \text{at crack formation} \tag{15a}$$

$$R_{d,y}(\gamma) = R_d(\gamma; D_f = 1) \qquad \text{at yielding} \tag{15b}$$

$$R_{d,u}(\gamma) = R_d(\gamma; D_f = 2) \qquad \text{for the ultimate state} \tag{15c}$$

Apparently, the corresponding optimal tuning ratios are $\gamma_p^*(D_f = D_c)$, $\gamma_p^*(D_f = 1)$, and $\gamma_p^*(D_f = 2)$. Although these values cannot minimize R_d at other states in a precise sense, time-history analysis suggests reasonable tuning. To obtain the constant tuning ratio γ_p^* in Eq. (7), a reference ductility factor denoted by $D_{f,\mathrm{ref}}$ must be determined in some way. Figure 8(a) shows that a $D_{f,\mathrm{ref}}$ ranging from 0.5 to 3.0 makes $R_{d,y}$ equal $R_{d,c}$, which means that minimizing $R_{d,y}$ leads to an approximately minimized $R_{d,c}$. Solving the following equation gives approximately minimized $R_{d,y}$ and $R_{d,c}$:

$$D_{f,\mathrm{ref}}^* = \arg\min R_{d,y}(D_{f,\mathrm{ref}}) \qquad \text{where} \quad 0.5 \le D_{f,\mathrm{ref}} \le 3 \tag{16}$$

Equation (15b) imposes $D_{f,\mathrm{ref}}^* = 1$. As $R_{d,u}$ gradually approaches $R_{d,y}$ for larger $D_{f,\mathrm{ref}}$ values (Fig. 8(b)), both $R_{d,u}$ and $R_{d,y}$ become large. Therefore, $D_f = 1$ could be a reasonable criterion for obtaining the tuning ratio in Eqs. (7) and (8).

4. TMD CONTROL DESIGN USING PERFORMANCE DIAGRAMS

4.1 Performance curves based on nonlinear time-history analysis

In practical engineering, control performance diagrams are useful tools for designing dampers in passively controlled buildings. We thus consider performance diagrams along with the critical constraints discussed in Section 3.2. The proposed diagrams can avoid time-history analyses with trial and error, giving a comprehensive understanding within a design parameter space. The control performance diagrams also visualize the relationship between $R_d(=\max U / \max U_0)$ and the normalized TMD deformation $\chi R_d(=\max d / \max U_0)$ with variations of the tuning parameters μ and h_a.

Consider a standardized acceleration spectrum S_a and standardized velocity spectrum S_v. The control performance diagram depends on whether the equivalent natural period at peak displacement T_{eq} belongs to the region of constant S_a or constant S_v (Fig. 2). Minor variations in the natural period T_{eq} do not affect the performance curves. The initial natural period is therefore set to 0.3 s for the constant

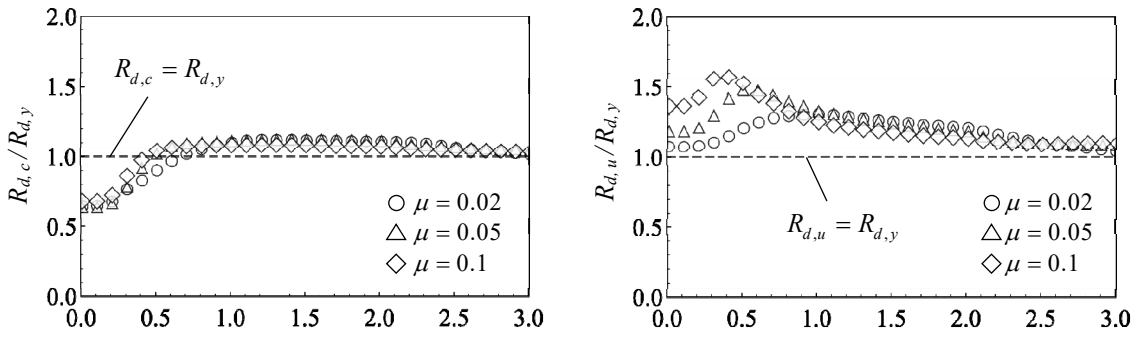

(a) Crack and yielding (b) Ultimate state and yielding

Fig. 8 Variations in reduction ratios

S_a case and 0.6 s for the constant S_v case. These two properties correspond to the five and ten-story buildings, respectively.

While the mass ratio μ and damping ratio h_a are changed continuously, the building and TMD deformations obtained by solving Eq. (2) can create the performance curves shown in Fig. 9. Despite the assumption of $D_f = 1$, these diagrams are applicable to a wide range of D_f values, as discussed in Section 3.2. In each graph, the thick curve at the top of the mesh refers to the optimal damping ratio h_a^* according to each mass ratio. A larger damping ratio than the optimum significantly reduces TMD deformation (χR_d) and slightly increases the reduction ratio R_d. In contrast, increasing the mass ratio μ is the only way to reduce R_d. To reduce TMD deformation, two methods are available: (1) increase μ or (2) increase h_a. If the TMD mass is to be as small as possible, increasing the damping constant is better; the reason for this is that the reduction ratio R_d becomes slightly higher as the TMD deformation decreases. However, an excessive damping ratio compared to the optimum significantly worsens control performance. The condition $h_a = 3h_{a,e}^*$ is an extreme case, which is depicted by the thick bottom curves in Fig. 9. In the range where the mass ratio is small, the change in TMD deformation as mass ratio increases is larger than the reduction ratio. As mentioned earlier, this visualization approach allows for better understanding of these trends.

4.2 Graphical approach to control design

Under the given structural building properties, a TMD can be designed using the following steps.

Step 1: Compute the effective mass M_b^{eff} of the controlled building. Set the constraints involving the allowable mass ratio $\hat{\mu}$, damping ratio $\hat{h}_a$, and deformation $\hat{d}$ for the TMD.

Step 2: Evaluate the stiffness ratio p_y and strength ratio τ. The direct method uses a push-over analysis of the frame model to obtain its envelope curve. The obtained round-shaped envelope is approximately replaced with a trilinear shape to obtain p_y and τ. Alternatively, these analyses can be avoided, and these ratios can be assumed to be 0.3.

Step 3: Obtain the inter-story drift angle (IDA) and the peak rooftop displacement $\max U_0$ by using the capacity spectrum method. Calculate the maximum allowable deformation ratio $\hat{\chi}$ from $\hat{d} / \max U_0$.

Step 4: Decide on the required reduction ratio ${}_{\text{req}}R_d$ so that the above IDA decreases below tolerance, such as IDA ≤ 1/100 rad.

Step 5: Draw the allowable region defined by ${}_{\text{req}}R_d$ and $\hat{\chi} \cdot {}_{\text{req}}R_d$ along with the constraints of the mass ratio $\hat{\mu}$ and damping ratio $\hat{h}_a$. Then, determine the design point inside the allowable region. For mid-rise buildings, the constraint $\hat{h}_a$ may be inactive, where h_a can be the optimum according to Eq. (10). If the allowable region does not exist in the control performance diagram, some constraints should be relaxed until the TMD properties can be found. Otherwise, consider another vibration control method besides a TMD.

Step 6: Compute the optimal tuning ratio γ_p^* from Eq. (7) using μ and structural properties including τ and p_y.

Step 7: Obtain the TMD mass m_a using the determined μ and the effective mass M_b^{eff}. Then, get the TMD properties k_a and c_a from Eq. (5) and Eq. (9).

Step 8: Conduct time-history analysis using the TMD properties and check whether the reduction ratio R_d and TMD deformation d are acceptable. If R_d is insufficient, the mass m_a should be increased; if d does not satisfy the constraint, the damping coefficient c_a should be increased. Then, perform time history analysis again.

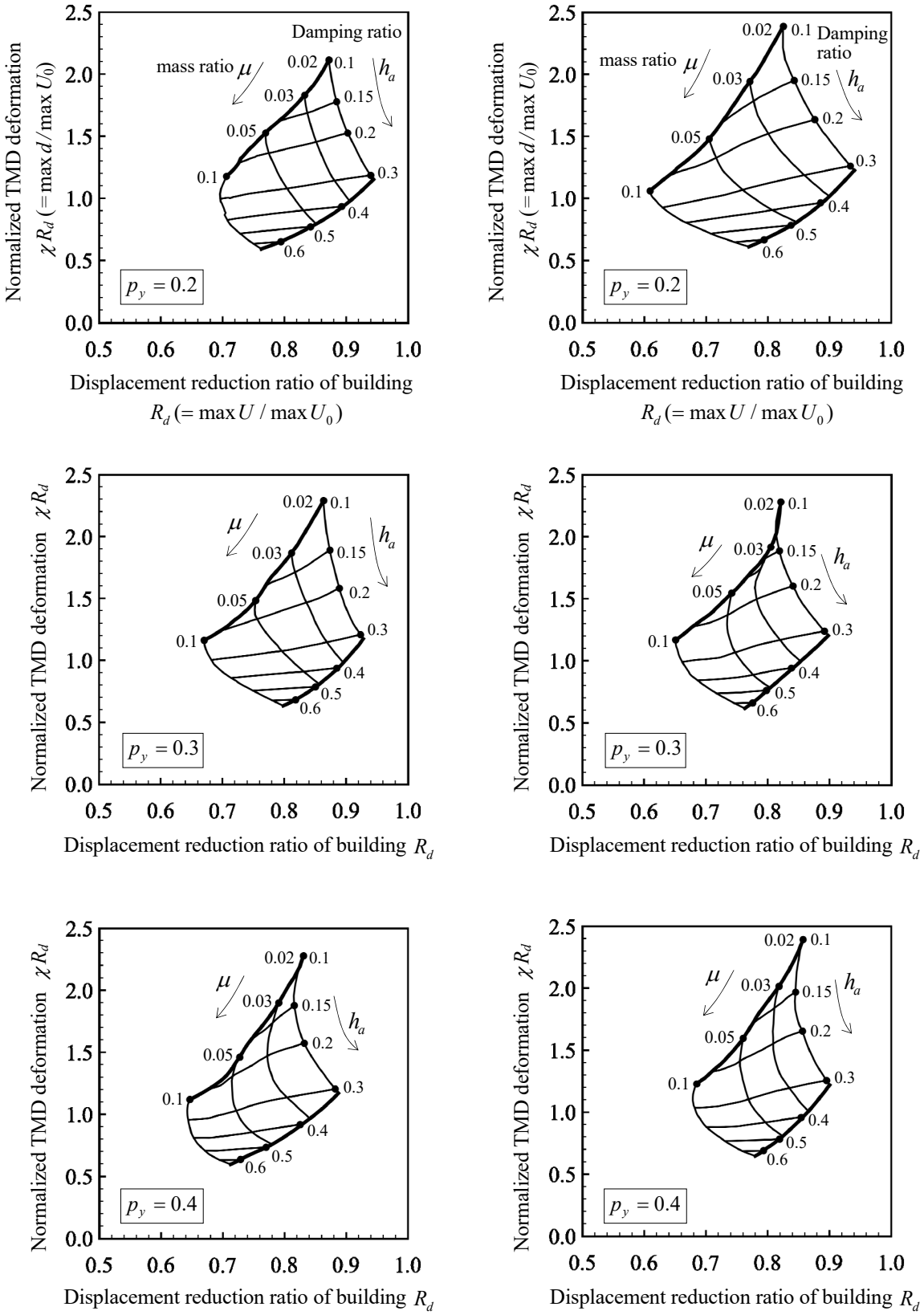

(a) Constant spectral acceleration domain (b) Constant spectral velocity domain

Fig. 9 Control performance diagrams

5. CONTROL DESIGN EXAMPLES FOR MID-TO-HIGH RISE BUILDINGS

5.1 Controlled buildings and ground motions

We demonstrate our methods with three mid-to-high rise buildings with five, ten, and 14 stories. These buildings are tower housing buildings compiled in the database of the Japan Building Disaster Prevention Association[13]. As shown in Fig. 10, the structural properties in the two horizontal directions are almost the same, and no torsional vibrations occur. The calculated safety factors for lateral load-carrying capacity are 1.13 for the five-story building, 1.06 for the ten-story building, and 1.06 for the 14-story building.

Table 1 lists recorded ground motions, in which peak ground velocity (PGV) is scaled to between 0.20 and 0.75 m/s for input motions. Figure 11 shows the response spectra of the scaled ground motions with a 0.5 m/s PGV.

5.2 Numerical modeling and spatial frame analysis

Spatial frame analysis was conducted using frame models instead of the lumped mass model. The

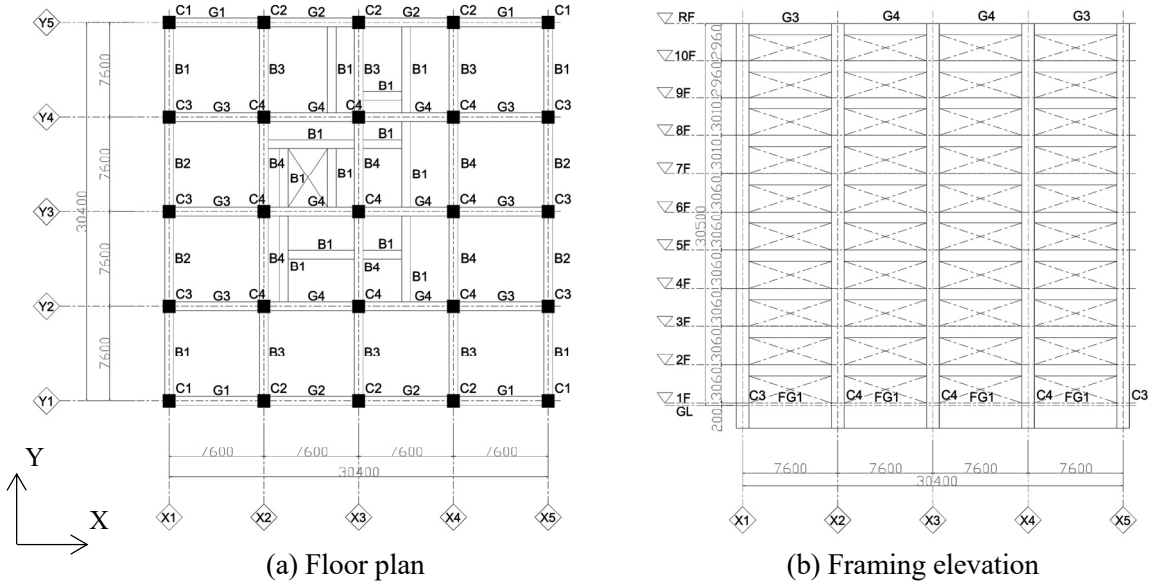

(a) Floor plan (b) Framing elevation

Fig. 10 Schematic diagram of the ten-story housing building with a TMD[13]

Table 1 Recorded ground motions

Earthquake	Dir.	PGA (m/s^2)	PGV (m/s)
El Centro 1940	NS	3.417	0.335
	EW	2.101	0.369
Taft 1952	NS	1.527	0.157
	EW	1.759	0.177
Hachinohe 1968	NS	2.297	0.344
	EW	1.802	0.378
JMA Kobe 1995	NS	8.180	0.965
	EW	6.174	0.803

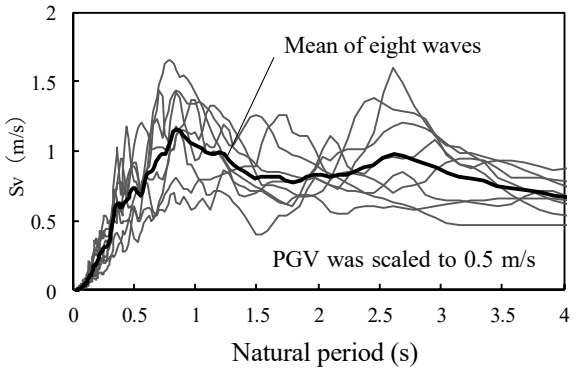

Fig. 11 Response spectra of recorded ground motions (0.05% damping ratio)

centralized TMD damping force may cause localized damage in the upper stories. In this case, the large TMD increases the axial force, especially in the top columns, which leads to a change in their strength. The frame models consisting of nonlinear members can simulate these effects.

This analysis employed a fiber model with axial force and bending moment interaction for the columns and a plastic-hinge model for the beams. The modeling of the beam-column joints and T-shaped beam width, including a part of the concrete floor, was based on the Architectural Institute of Japan Standard for Structural Calculation of Reinforced Concrete Structures[14]. The floor diaphragms are considered rigid. Total designed TMD mass was distributed at nine nodal points over the rigid rooftop (intersections of X2, X3, X4 and Y2, Y3, and Y4 base lines shown in Fig. 10(a)). The structural analysis program RESP-D ver. 3.1.1 was used to conduct time history analysis[15].

5.3 Tuning TMDs using control performance diagrams

The maximum allowable values are 0.05 for the mass ratio μ, 0.3 for the damping ratio h_a, and 0.5 m for the TMD deformation. First, incremental static analysis was carried out to construct the equivalent SDOF system using the uncontrolled buildings without TMDs. Table 2 lists the obtained natural periods and parameters τ and p_y. Then, the tuning parameter was found using the control performance diagram so that the reduction factor was below 0.85.

As an example, we will outline the design procedure for the ten-story building. The first step was to draw the allowable region in the control performance diagram. To obtain the upper limit, we used three assumptions: (1) each story yields at an IDA of 1/150 rad; (2) the ductility factor is 1.0; and (3) the height of the building is 30 m. The top floor displacement $\max U_0$ then became 0.2 m by multiplying the three values: 1/150 rad, 1.0, and 30 m. For a ductility factor of 2.0 during more severe responses, the TMD deformation should be below 0.5 m. Because the rooftop displacement reaches 0.4 m, the vertical axis value should be below 1.25 ($\hat{d} / \max U_0$). In Fig. 9, setting the parameters μ to 0.05 and h_a to 0.25 satisfies both the constraints and required R_d.

For the 14-story building with a height over 31 m, the same tuning parameters give a TMD deformation of 0.34 m (1/150 rad $\times 1.0 \times 3.0 \times 14 \times 1.2$) for $D_f = 1$ and 0.68 m for $D_f = 2$. This result implies that a long-stroke damper or a stopper is needed to prevent excessive strokes. For the five-story building, the optimal damping ratio of $h_a = 0.14$ could be selected because the TMD deforms within a small range. Table 2 lists the tuned parameters along with the structural properties of each building.

5.4 Peak responses of buildings and TMDs

Table 3 compares the predicted results with the time history analyses. The prediction errors are 19% for the TMD deformation and 7% for R_d (or the building displacement). In this case, an average ductility

Table 2 Properties of controlled buildings and TMDs

Building				TMD					
Stories	Fundamental natural period (s)	Stiffness ratio* p_y	Strength ratio** τ	Mass ratio μ	Tuning ratio γ	Damping ratio h_a	Mass m_a (t)	Stiffness k_a (kN/m)	Damping coefficient c_a (kNs/m)
5	0.36	0.30	0.37	0.05	0.56	0.14	178	2.03×10^4	0.52×10^3
10	0.62	0.33	0.31		0.57	0.25	363	1.30×10^4	1.09×10^3
14	0.75	0.32	0.27		0.55		507	1.15×10^4	1.21×10^3

* p_y: normalized secant stiffness at yielding divided by initial stiffness for equivalent SDOF building
** τ: the first strength divided by the second strength in the trilinear envelope of the SDOF building

factor D_f of 1.0 equals the value used in making the control performance diagrams. Figure 12 demonstrates the cause of the errors. In the top graphs, a good control performance was achieved, and no localized damage was confirmed. Although the TMD did not reduce the building response in the bottom graphs (for El Centro EW, Taft EW, and Hachinohe NS), the uncontrolled building response was extremely small compared to the previous case. This result implies that these three cases fell into local minima on the non-smoothed response spectrum curves, where viscous damping is quite ineffective even in elastic systems. Removing these special cases gives an average R_d of 0.78, which is almost equal to the predicted value ($R_d = 0.8$). The TMD reduced the maximum inter-story drift to below 1/100 rad except in the case of the JMA Kobe NS input. Table 4 lists the R_d for the typical PGV, and Fig. 13

Table 3 Accuracy of predicted peak responses

	Input ground motions								Mean values	Predicted values	Predicted / Mean
	El Centro		Taft		Hachinohe		JMA Kobe				
	NS	EW	NS	EW	NS	EW	NS	EW			
D_f	0.98	0.74	0.74	0.78	0.91	1.38	1.20	1.31	1.00	-	-
d / U_0	1.50	1.76	1.26	1.47	1.40	1.64	1.43	1.47	1.49	1.20	0.81
R_d	0.69	0.96	0.76	1.08	0.89	0.85	0.79	0.79	0.85	0.79	0.93

d: peak deformation of TMD; U_0: rooftop displacement for uncontrolled building; R_d: displacement reduction ratio; D_f: q/q_y, where q_y is the yielding displacement for a SDOF building and q is modal displacement; R_d: normalized peak controlled response divided by uncontrolled response over distributed inter-story drift

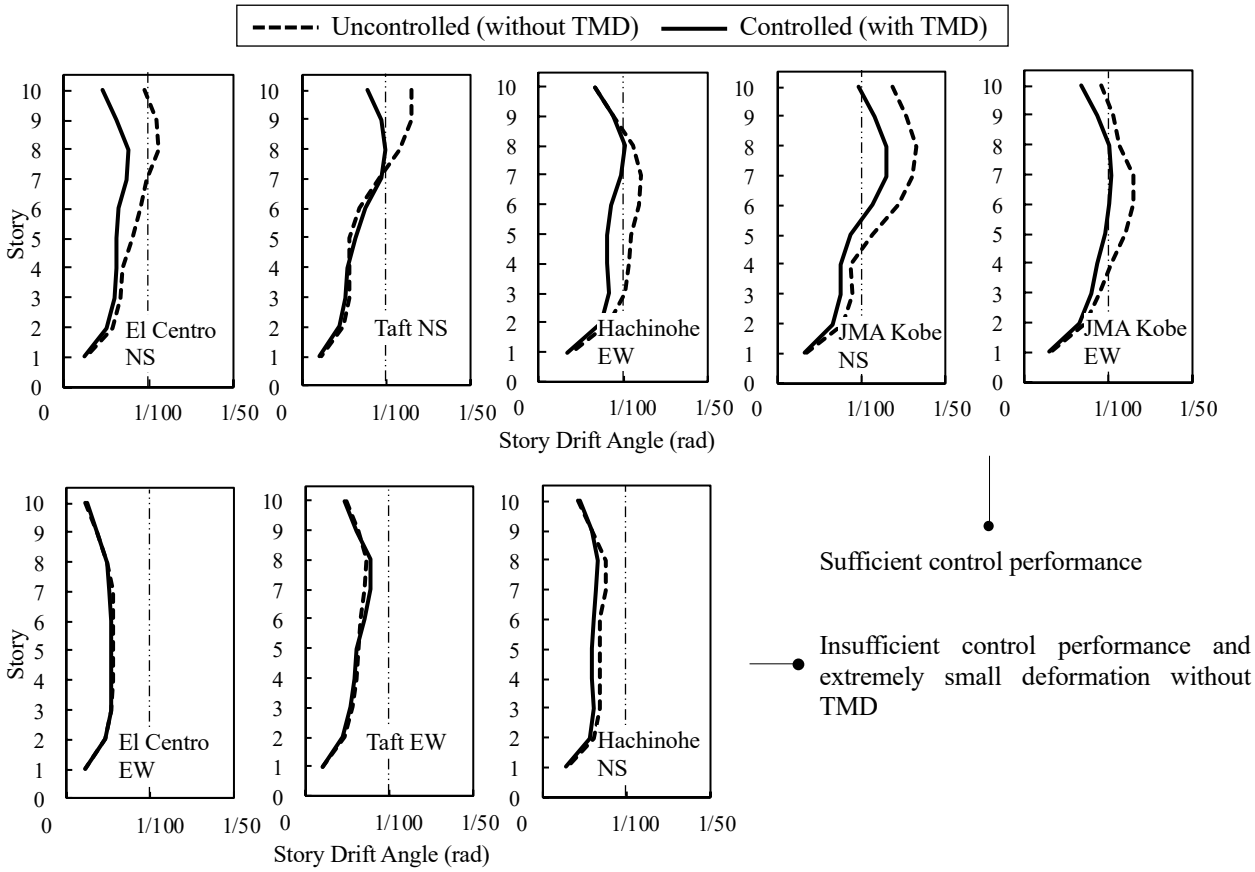

Fig. 12 Control performance in terms of peak story drift angles (PGV = 0.5 m/s, ten-story building)

shows the variations of R_d in terms of PGV. These results demonstrate that the reduction ratio R_d ranges from 0.80 to 0.85. Figure 14 indicates that the TMD deformation d satisfies the constraints ($d < 0.5$ m) even for the severe input (PGV = 0.75 m/s). In the 14-story building, some ground motions deformed the TMD beyond its constraints. To prevent the damage, adding a stopper device to the TMD was effective without reducing control performance. Figure 15 shows the maximum IDA of all the stories in the controlled and uncontrolled buildings. Apparently, the enveloped IDA of the eight inputs was reduced to less than the average. For example, the PGV corresponding to an IDA of 1/100 rad was 0.4 m/s for the uncontrolled case and 0.6 m/s for the controlled case. It was also confirmed that the acceleration reduction from the TMD was roughly 0.95 for the five-story building and 0.85 to 0.90 for the ten and 14-story buildings, respectively. The TMDs did not amplify the top acceleration.

Table 4 Reduction ratios of peak responses in controlled buildings

PGV (m/s)	Input ground motions								Mean values	Standard deviation
	El Centro		Taft		Hachinohe		JMA Kobe			
	NS	EW	NS	EW	NS	EW	NS	EW		
0.25	0.64	0.80	0.72	0.88	0.90	0.70	0.83	0.80	0.78	0.09
0.50	0.69	0.96	0.76	1.08	0.89	0.85	0.79	0.79	0.85	0.12
0.75	0.68	0.94	0.64	0.90	0.89	0.89	1.00	0.82	0.85	0.13

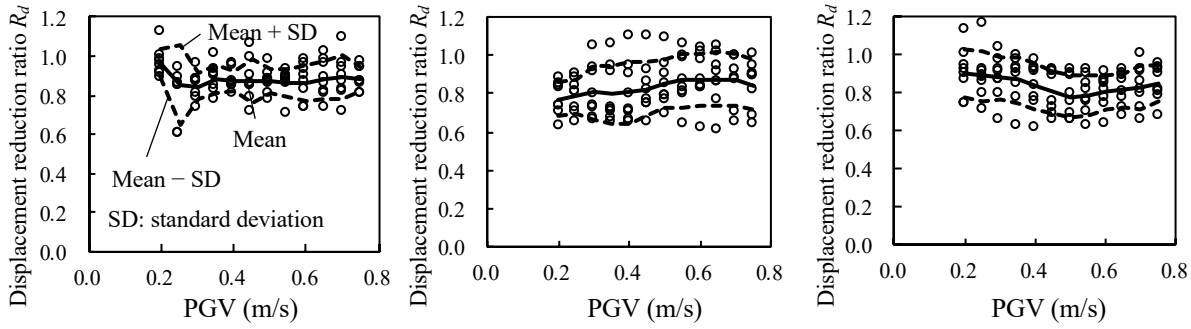

(a) Five-story building (b) Ten-story building (c) 14-story building

Fig. 13 Variations in control performance in terms of PGV

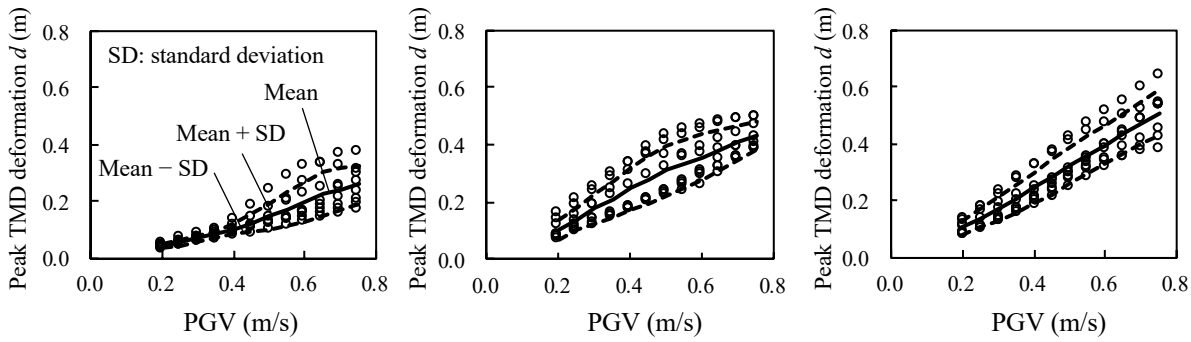

(a) Five-story building (b) Ten-story building (c) 14-story building

Fig. 14 Variations in TMD peak deformation in terms of PGV

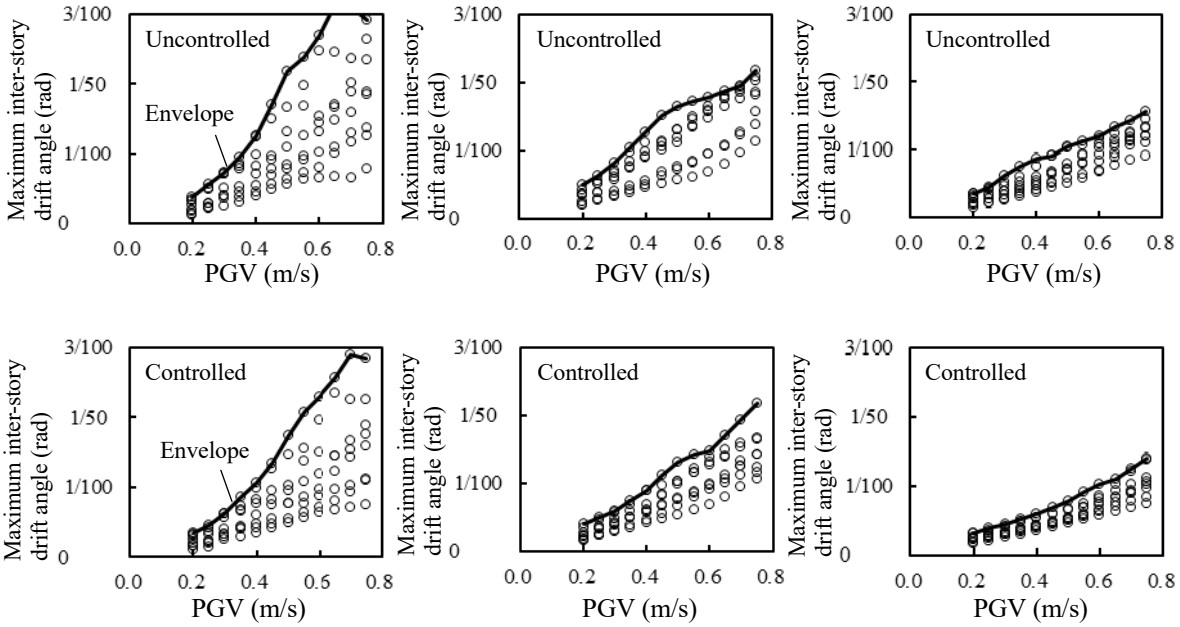

(a) Five-story building (b) Ten-story building (c) 14-story building

Fig. 15 Variations in peak IDA in terms of PGV

6. CONCLUSIONS

In this study, we created control performance diagrams using time history analysis to support tuned mass damper (TMD) design for middle- and high-rise reinforced concrete buildings. The methods were demonstrated, and the effect was verified with frame analysis. The findings are summarized below.

- For a building ductility factor (D_f) above 1.0, the TMD to building deformation ratio approximately holds. Therefore, the control performance curve based on $D_f = 1$ is applicable to a wide range of D_f values, giving the predicted TMD deformation.
- By optimizing the TMD for the seismic intensity at which the building ductility factor is 1.0, its performance at reducing building displacement approximately holds for more severe ductility factors. A TMD with a 5% mass ratio reduces peak building displacement by 15% to 20%.
- Control performance diagrams are useful, especially with multiple active constraints, including the allowable mass, damping ratio, and TMD deformation.
- Predicted values from the controlled performance curves have good accuracy compared to the results of three different buildings through spatial frame analysis.
- The large damping force of TMDs reduces the overall inter-story drift without any localized deformation of the building.

ACKNOWLEDGMENT

This work was conducted with the support of the Obayashi Foundation. The authors are grateful to Yutaro Sumi, Naoya Goto, and Ning Jiao for promoting the seismic rehabilitation techniques of existing buildings using TMDs in Taiwan.

REFERENCES

1) Sone, T., Ogino, K., Kamoshita, N. and Muto, K.: Experimental Verification of a Tuned Mass Damper System with Two-Phase Support Mechanism, *Japan Architectural Review*, Vol. 2, No. 3, pp. 250–258, 2019.
2) Nakai, T., Kurino, H., Yaguchi, T. and Kano, N.: Control Effect of Large Tuned Mass Damper Used for Seismic Retrofitting of Existing High-Rise Building, *Japan Architectural Review*, Vol. 2, No. 3, pp. 269–286, 2019.
3) Ishikawa, Y., Maseki, R., Aono, S., Kimura, Y. and Yamato, N.: Development and Analysis of Long Stroke Tuned Mass Damper for Earthquakes, *Japan Architectural Review*, Vol. 2, No. 3, pp. 259–268, 2019.
4) Kano, N., Hori, Y. and Kurino, H.: Analytical Study on Tuned Mass Dampers for RC High-Rise Building with Structural Period Fluctuation—Part1 Fundamental Study on Optimal Settings of Dual TMDs, *Summaries of Technical Papers of Annual Meeting Architectural Institute of Japan*, B-2, pp. 695–696, 2015 (in Japanese).
5) Kaneko, K.: Multipurpose Passive Control of Mid-Story Isolation Buildings Designed to Mitigate Seismic Response in Substructure, *Journal of Structural and Construction Engineering* (*Transactions of AIJ*), Vol. 80, No. 718, pp. 1869–1879, 2015 (in Japanese).
6) Kaneko, K.: Tuning Strategy of Hysteretic Mass Damper for Reducing Inter-Story Drift beyond Elastic Limit of Steel Buildings, *Journal of Structural and Construction Engineering* (*Transactions of AIJ*), Vol. 83, No. 752, pp. 1423–1433, 2018 (in Japanese).
7) Lin, P. Y., Lin, T. K. and Hwang, J. S.: A Semi-Active Mass Damping System for Low- and Mid-Rise Buildings, *Earthquakes and Structures*, Vol. 4, No. 1, pp. 63–84, 2013.
8) Lin, G. L., Lin, C. C., Lu, L. Y. and Ho, Y. B.: Experimental Verification of Seismic Vibration Control Using a Semi-Active Friction Tuned Mass Damper, *Earthquake Engineering and Structural Dynamics*, Vol. 41, No. 4, pp. 813–830, 2012.
9) Kaneko, K. and Takahashi, K.: Optimal Tuning Ratio of Mass Damper in Reinforced Concrete Buildings Subjected to Strong Ground Motion, *Journal of Structural and Construction Engineering* (*Transactions of AIJ*), Vol. 85, No. 777, pp. 1387–1395, 2020 (in Japanese).
10) Nakai, T. and Kurino H.: Proposition of Semi-Active Controlled Tuned Mass Damper Adaptable to a Structure's Period Fluctuation, *Journal of Structural and Construction Engineering* (*Transactions of AIJ*), Vol. 83, No. 744, pp. 233–243, 2018 (in Japanese).
11) Takeda, T., Sozen, M. A. and Nielsen, N. N.: Reinforced Concrete Response to Simulated Earthquake, *Journal of Structural Division ASCE*, Vol. 96, pp. 19–26, 1970.
12) Warburton, G.: Optimum Absorber Parameters for Various Combinations of Response and Excitation Parameters, *Earthquake Engineering and Structural Dynamics*, Vol. 10, pp. 381–401, 1982.
13) Japan Building Disaster Prevention Association: Typical Design Examples of Buildings, 628 pp., 2007 (in Japanese, title translated by the authors).
14) Architectural Institute of Japan: AIJ Standard for Structural Calculation of Reinforced Concrete Structures, 560 pp., 2018 (in Japanese).
15) Kozo Keikaku Engineering: Structural Analysis Program for Buildings RESP-D Analysis User's Manual, 294 pp., 2019 (in Japanese, title translated by the authors).

(Original Japanese Paper Published: August, 2021)
(English Version Submitted: February 28, 2022)
(English Version Accepted: March 19, 2022)